

Resolving Orographic Rainfall On The Indian West Coast

K. Suprit and D. Shankar

National Institute of Oceanography, Dona Paula, Goa, India.

Corresponding Author:

K. Suprit

National Institute of Oceanography,

Dona Paula, Goa, India.

PIN: 403004

E-mail: suprit.kumar@gmail.com

Short title:

Resolving Orographic Rainfall On The Indian West Coast

Accepted Preprint:

This is a preprint of an article in International Journal of Climatology (in press) published online in Wiley InterScience (www.interscience.wiley.com) DOI: 10.1002/joc.1566.

ABSTRACT

We discuss a method to obtain the spatial estimates of rainfall on the Indian west coast for calculating the surface water budget. The region includes the basin of the Mandovi River, a typical west-coast river whose catchment area includes the Sahyadris range. The rainfall maps obtained by a multivariate interpolation scheme, with elevation as the third variable, were able to capture the sharp increase in rainfall on the windward slopes and the exponential decay in rainfall on the leeward side. The rainfall maps were used to force a hydrological model and the simulated discharge was within 16% of the observed discharge in 16 of 18 years during 1981–1998; the average error over the 18 years was 8%, which is much less than the estimated error of ~15–20% in the observed discharge. The Mandovi river discharge provided a reliable and independent validation of the accuracy of the rainfall estimate as the river is purely rain-fed. The method provides a better estimate of rainfall in the Mandovi basin, and therefore for the Indian west coast, than existing rainfall datasets. The key result is that treating the windward and leeward sides separately by an *a priori*, subjective extraction of the ridge line can reduce the underestimation of rainfall that is common in mountainous terrain when the data coverage is sparse.

Keywords: Hydrological modelling, Multivariate interpolation, Orographic rainfall, Ridge, Sahyadris, Western Ghats, Freshwater discharge, Mandovi River, Salinity, Indian Ocean.

1. INTRODUCTION

The crucial role of rivers in the global freshwater budget and climate has led to the assembling of global databases on river discharge (Vörösmarty *et al.*, 1996; Graham *et al.*, 1999) and the development of numerical models to simulate river discharge on continental scales (Coe, 1998, 2000). In the north Indian Ocean too, the importance of river discharge for the thermodynamics of the upper ocean (Han *et al.*, 2001; Howden and Murtugudde, 2001; Shenoi *et al.*, 2002) and low-frequency variability of sea level along the Indian coast (Shankar and Shetye, 1999; Shankar, 2000; Shankar and Shetye, 2001; Han and Webster, 2002) has been highlighted, but there is a dearth of information on river discharge (Shankar *et al.*, 2004), leading, at times, to attempts to determine the discharge through inverse modelling (Yaremchuk *et al.*, 2005).

The two rainfall maxima in the north Indian Ocean are in the north-eastern Bay of Bengal (adjoining the west coast of Myanmar (Burma)) and the eastern Arabian Sea (adjoining the west coast of India), and orography plays a role in concentrating the rainfall in these regions (Sarker, 1966; Xie *et al.*, 2006). The high rainfall is matched by high freshwater discharge from rivers, making the river discharge crucial for determining the near-surface salinity and temperature (Han *et al.*, 2001; Howden and Murtugudde, 2001). The difference between the northern bay and the eastern Arabian Sea lies in the scale of rivers involved: the rivers draining into the former are the big rivers of the Indian subcontinent, but those draining into the latter are small (except the Tapi and the Narmada). Among the big rivers draining into the bay are the Ganga and the Brahmaputra, whose discharge is the fourth largest in the world (Martin *et al.*, 1981; Fekete *et al.*, 2000). Hence, these rivers draining into the bay are better gauged than the small rivers draining through the Indian west coast into the eastern Arabian Sea.

The most striking feature of the Indian west coast is the presence of the Sahyadris range (Western Ghats), which runs parallel to the coast (Figure 1). The coast itself is narrow, no more than a few tens of kilometres wide and extending up to the foothills of Sahyadris. From the foothills, the slopes of the Sahyadris rise abruptly in the form of an escarpment to an average elevation of 700 m. At several places, the escarpment is broken by river valleys. The axis of the range lies perpendicular to the prevailing summer-monsoon winds. The moisture-laden monsoon winds cause heavy rainfall on the windward side of the range, distinguishing it from the much drier leeward side (Figure 2). Most of the west-coast rainfall (~90%) occurs during June–September, there being negligible rainfall during December–April.

The small area and mountainous terrain of the west coast make it difficult to impound water, leading to a large fraction of the heavy summer-monsoon rainfall flowing into the eastern Arabian sea. The large number of rivers and their small scale has ensured that many of them have no discharge gauges. This makes hydrological modelling the only viable tool for estimating the potentially large freshwater discharge into the eastern Arabian Sea. Salinity data from the region often show rapid changes in near-surface salinity as the surface waters are advected by the large-scale alongshore current (Shankar *et al.*, 2005); potential implications for air-sea coupling imply

there is a need for a discharge data set that captures the high alongshore spatial variation that is a natural consequence of the small scale of these west-coast rivers.

This need for estimating the freshwater discharge into the seas around India led Shankar *et al.* (2004) to assemble a framework for estimating river discharge. The framework was based on THMB (Terrestrial Hydrologic Model with Biogeochemistry), the numerical model developed by Coe (2000). (This model was earlier called HYDRA (HYDrological Routing Algorithm).) To demonstrate its viability, Shankar *et al.* applied the framework to the Mandovi, a river in Goa on the Indian west coast (Figure 1). Strictly, Mandovi is the name of only the estuary, Mhadei being the name of the freshwater stream (Shetye *et al.*, 1995). In this paper, however, we use "Mandovi" for the river also. Shankar *et al.* assumed that a framework that works for the Mandovi would work as well for the other, similar rivers draining into the eastern Arabian Sea. The Mandovi is typical of the rivers along the Indian west coast. It is totally rain-fed and small (length 87 km, basin area 2032 km² (Rao, 1975)). It is one of the best-studied estuaries in India. It is also one of the few that has a discharge gauge. This gauge is located at Ganjem (Figure 1), about 50 km from the mouth and just upstream of the limit of tidal incursion in the estuary (Shetye *et al.*, 1995). Another discharge gauge is located at Kulem on the Khandepar, the biggest of the Mandovi's tributaries (Figure 1). Five rain gauges are located in the basin. One of them, at Panaji, is situated at the mouth; the easternmost (and therefore highest) rain gauge is at Gavali. The other three gauges are located at Mhapsa, Valpoi, and Asoga (Figure 1).

Dense sampling in such mountainous terrain shows high spatial variability of rainfall (Frei and Schar, 1998). The low number of gauges in the Mandovi basin (typical of river basins on the Indian west coast) makes it difficult to map the rainfall into a grid suitable for THMB. As noted by Daly (2006), in regions with a terrain as complex as on the Indian west coast, there is no satisfactory method for quantifying the errors associated with spatial data sets; the best approach is to involve different and independent data sets combined with common sense to estimate the spatial variation. The rain gauges, which permit us to derive spatial estimates of rainfall, and the discharge gauges provide us two independent data sets. In this paper, we test existing rainfall data sets and present a new one for the Mandovi basin. We show that the existing rain gauges can be used to estimate the annual discharge to within 15% of the measured values if the rainfall-mapping algorithm accounts for the elevation in addition to horizontal position: the key lies in treating the windward and leeward sides separately by specifying the ridge. Since the Mandovi is typical of the small rivers flowing down from the Sahyadris into the eastern Arabian Sea, the method can be extended to other rivers on the Indian west coast.

We begin (in Section 2) by showing that existing rainfall data sets, when used to force THMB, result in discharge estimates that differ considerably from the Ganjem measurements. A Cross-Validation procedure for estimating rainfall is presented in Section 3 and it is applied to the Mandovi basin in Section 4. Section 5 concludes the paper.

2. TESTING EXISTING RAINFALL DATA SETS

There exist a few rainfall data sets for the Indian subcontinent and we first checked if they yielded discharge estimates comparable to those observed at Ganjem. This was done using the discharge simulation framework assembled by Shankar *et al.* (2004). We begin with a brief description of this framework and then use it to test the existing rainfall data sets.

2.1. Discharge simulation framework

The framework of Shankar *et al.* (2004) had at its core the hydrological routing algorithm called THMB (Coe, 2000). Given the distribution of local rainfall and evapo-transpiration, THMB can route the surface run-off and sub-surface run-off (also called sub-surface drainage or baseflow) to its destination, the sea or an inland lake. It uses a linear reservoir model to simulate water transport in terms of local flow directions derived from the local topography, residence times within a grid cell, and effective flow velocities. The water transport is represented by the time-dependent change of three water reservoirs. The first is the river water reservoir (W_r), which contains the sum of upstream and local water in excess of that which is required to fill a local surface water depression; the second reservoir is the surface run-off pool (W_s), which contains water that has run off the surface locally and is flowing towards a river; the third reservoir is the sub-surface runoff pool (W_d), which contains water that has drained through the local soil column and is flowing towards a river. The water entering the hydrological network is the sum of the land surface run-off (R_s), sub-surface drainage (R_d), and the flux of water from upstream grid cells (F_{inp}); rainfall and evaporation over the water surface (Coe, 2000) was neglected by Shankar *et al.* (2004) because there is no significant water body in the Mandovi basin.

The flow is governed by three differential equations (Coe, 2000):

$$\frac{dW_s}{dt} = R_s - \frac{W_s}{T_s} \quad (1a)$$

$$\frac{dW_d}{dt} = R_d - \frac{W_d}{T_d} \quad (1b)$$

$$\frac{dW_r}{dt} = \left(\frac{W_s}{T_s} + \frac{W_d}{T_d} \right) - \frac{W_r}{T_r} + \sum F_{inp} , \quad (1c)$$

where T_s , T_d , and T_r denote the residence times of water in their respective reservoirs. (The reservoirs are expressed in m^3 , the residence times in seconds, and the surface and sub-surface runoffs and F_{inp} in m^3/s .) Following Coe (2000) and Shankar *et al.* (2004), the first two residence times were considered constant for simplicity. T_r is a ratio of resolution and effective velocity of water, which is parameterized differently for different grid cells (see Coe (2000) for more details). The model equations were integrated forward in time using an explicit differencing scheme; the model time step was 5 minutes.

THMB requires the following inputs: a DEM (Digital Elevation Model) to map the topography, and surface run-off and sub-surface runoff for each grid cell.

A freely available DEM called GLOBE (Global Land One Kilometre Base Elevation) (GLOBE, 2004), with a resolution of 30 arc seconds (~1 km), was used by Shankar *et al.* (2004), who demonstrated the framework by applying it to the Mandovi River in Goa (Figure 1). Over a large fraction of its length, the Mandovi is much less than a kilometre wide. A DEM cannot represent the surface topographic features smaller than its resolution; hence, the GLOBE DEM failed to resolve the narrow river valleys in the Mandovi basin, and local flow directions derived from it were inaccurate. Therefore, Shankar *et al.* (2004) developed a set of tools based on a Geographic Information System (GIS) called GRASS (Geographical Resources Analysis Support System) GIS (Neteler and Mitasova, 2002) to edit the DEM manually (Kotamraju and Shankar, 2004) so that the river could be represented accurately in the model. The modified DEM was able to resolve the river basin accurately: the area of the basin was estimated to be 1896 km², within 10% of previously published estimate of 2032 km² (Rao, 1975). The catchment area at Ganjem was estimated at 872 km², just 1% less than the estimate of the Central Water Commission (CWC, river discharge data). (High-resolution DEMs like SRTM (Shuttle Radar Topography Mission; resolution 3 arc seconds) (USGS, 2004) also show similar routing problems (and therefore require editing) at least when they are averaged to a 30-arc-seconds grid.)

Shankar *et al.* (2004) used rainfall and evapo-transpiration data from the NCEP/NCAR (National Center for Environmental Prediction/National Center for Atmospheric Research) Reanalysis (Kalnay *et al.*, 1996) and also rain-gauge data from Panaji and Valpoi in the Mandovi basin to demonstrate the viability of the framework. Following Coe (2000), they partitioned the difference between rainfall and evapo-transpiration (both of which they assumed to be uniform over the basin in the absence of a method to map the spatial variability) between surface run-off (30%) and sub-surface runoff (70%). Shankar *et al.* (2004) showed that global models like the one used for creating the NCEP/NCAR Reanalysis are incapable of resolving the orography of the Sahyadris (owing to a coarse resolution) and therefore considerably underestimate the rainfall in the Mandovi basin. In the NCEP/NCAR reanalysis, rainfall is a Class C variable (minimum impact of data assimilation) (Kalnay *et al.*, 1996) and has been shown to be unsuitable for climatic studies owing to large errors associated with the data (e.g. Janowiak *et al.*, 1998). Better results were obtained by Shankar *et al.* (2004) by using gauge data, but the in situ data had to be mapped to the uniform model grid; they showed that mapping the spatial variation of rainfall was critical for simulating the discharge at Ganjem.

2.2. Testing existing gridded data sets

Gridded rainfall data sets based on observations are now available at various spatial and temporal scales. Some of these data sets are based on rain-gauge measurements and some on satellite estimates; some of them use model-derived reanalysis data. We tested three available rainfall data sets to see if these rainfall data produced discharge estimates consistent with the

observations. In all cases, the evapo-transpiration was the same and was based on the NCEP/NCAR Reanalysis (Kalnay *et al.*, 1996); evapo-transpiration was assumed to be uniform over the basin. The discharge data at Ganjem and Kulem were obtained from CWC.

2.2.1 CRU data set. The Climate Research Unit's (CRU, University of East Anglia) CRU TS 2.0 is a widely used long-term data set for climatic variables. This data product consists of nine monthly climate variables gridded on a 0.5° grid; the product is based on surface meteorological observations (New *et al.*, 1999, 2000). The data are available on-line (Table I) for 1901–2000. The grids were constructed by interpolating various available observational data sets using a thin-plate spline interpolation scheme. We forced THMB with the monthly rainfall field from CRU. As with NCEP/NCAR, the rainfall forcing was assumed constant over the catchment. As there are four CRU grid cells that contain a part of the Mandovi basin (Figure 3), the rainfall from the cell with highest rainfall value was used to force THMB (the grid cell is marked by a solid dot in Figure 3). The simulated discharge was considerably less than the observed, the average error over 1981–1998 being 53% (Table II). The problem is the grid size, the area of a single CRU cell being larger than the Mandovi basin; hence, it was unable to resolve the rainfall variability in the basin.

2.2.2 IMD data set. Rain-gauge data in India are collected and maintained by the India Meteorological Department (IMD). IMD recently released a 1° gridded, daily rainfall data set for 1951–2003 based on these data (Table I) (Rajeevan *et al.*, 2006a,b). This data set was constructed by interpolating station data using Shepard's interpolation scheme, which is essentially an inverse-distance weighting scheme. The question is how well the IMD data set maps the west-coast rainfall. We tested it by forcing THMB with the IMD rainfall product. The Mandovi basin spread across two IMD cells, with each cell accounting for a part of the basin (Figure 3). The catchment upstream of Ganjem fell in the eastern cell (E), but the rainfall over this cell was much less than the rainfall over the western cell (W), in which fell the basin area downstream of Ganjem. We took this to be an artefact of the grid, with the eastern (western) cell with low (high) rainfall representing the leeward (windward) side of the Sahyadris. Hence, the rainfall data used to force THMB were taken from the western cell (W). The daily rainfall data were averaged to obtain monthly values for THMB. The estimated discharge (Table II) was better than the discharge simulated using the CRU data, but the errors were still unacceptably high (average error of ~44% over 1981–1998). The discharge was underestimated by the IMD rainfall, the error being larger in years with high discharge (and therefore high rainfall). Thus, the IMD data were unable to capture the large interannual variability inherent in the west-coast monsoon rainfall and the simulated discharge had a much lower variance than observed (Table II).

2.2.3 TRMM data set. The third rainfall data set we tested was TRMM (Tropical Rainfall Measuring Mission) (TRMM, 2006). We used TRMM data product 3B43 (Combined TRMM and other data sources), which combines calibrated satellite data (from TRMM and other satellite precipitation sensors) and ground-based global rain-gauge data sets to produce the “single, best-estimate data” (TRMM, 2006). The 3B43 rainfall data are available on-line on a 0.25° grid from January 1998 onwards. Since discharge measurements were available only till 1999, the TRMM

data set was tested only for two years, 1998 and 1999. The error in simulated discharge, and therefore in the TRMM rainfall estimate, was 75% for 1998 and 69% for 1999. As with the CRU and IMD data, TRMM also considerably underestimates rainfall over the basin.

Thus, of the three data sets tested, the best discharge estimates were obtained with the IMD data (though it had the lowest resolution) because it used in situ rain-gauge data. The problem with the IMD data set is that its objective was to map the rainfall over India, not just over its west coast. This led to the interpolation algorithm ignoring the effect of elevation and the need to ensure continuity led to the use of fewer rain gauges than were actually available for (say) the Mandovi basin.

3. NEW INTERPOLATION METHOD

3.1 Data

Using data for 4 years for 22 stations from the area around the Mandovi basin, Suprit and Shankar (2006) showed that it is possible to generate a rainfall data set that results in more accurate discharge estimates. Their study was limited, however, by the short length of the time series and that the rain-gauge data they used had not passed through the same level of quality checks that are mandatory in IMD.

Hence, we obtained daily rainfall data from the National Data Centre of IMD for 20 stations (Table III, Figure 1) around the Mandovi basin. From the daily data, monthly average rainfall for 1981–1998 was derived because both rainfall and discharge data were available for this period. Data on evapo-transpiration were taken from the NCEP/NCAR Reanalysis (Kalnay *et al.*, 1996) and, in the absence of any information on how it varies spatially within the basin, evapo-transpiration was assumed to be spatially uniform. As noted by Shankar *et al.* (2004), the NCEP/NCAR evapo-transpiration estimates match those of IMD. (See Rao *et al.* (1971) for the IMD estimates.) Hence, given that temperature and humidity data are even sparser than rainfall data, we used the NCEP/NCAR estimates for the THMB simulations.

3.2 Interpolation method

A good interpolation technique should not only be objective, but also subjective enough to use the already known facets of spatial distribution of rainfall in the complex terrain to complement the lack of data points. In general, a good rainfall map should fulfil the following criteria: It should be able to reproduce known spatial characteristics of rainfall (as it is known to a local observer), it should compare favourably with station rainfall, and it should be validated with independent criteria like water budget calculations.

We adopted the splines method, a variational technique, because it is more physically meaningful than statistical techniques (Mitas and Mitasova, 1999). Geostatistical methods like kriging were not chosen because of the need for subjective decisions (Journel, 1996): data in a data-sparse region like the Mandovi basin may not contain enough information about the important features to enable such subjectivity to succeed. The two methods, however, have been shown to be formally equivalent (Cressie, 1993).

Splines have been used extensively in the interpolation of various climate variables (see, for example, Hutchinson, 1995, 1998a,b; New *et al.* 1999; Hofierka *et al.* 2002; Jeffrey *et al.* 2001). An implementation of the multivariate spline interpolation method called “Regularized Spline with Tension” (RST) has been developed and incorporated within GRASS GIS (GRASS, 2006). The method has been applied successfully to regions having complex topography (Hofierka *et al.*, 2002). A detailed discussion of the mathematical formulation of the RST method is presented by Mitasova and Mitas (1993) and Hofierka *et al.* (2002).

The spline interpolation technique is based on the premise that the interpolation function should pass through or close to the data points while trying to remain as smooth as possible (Mitas and Mitasova, 1999). The scheme is able to capture a more complex, spatially variable relation between rainfall and elevation than the traditional methods based on statistical correlation (Hofierka *et al.*, 2002). The explicit form of RST function and solutions for undermined coefficients are given in Mitasova and Mitas (1993) and Hofierka *et al.* (2002). To interpolate rainfall with elevation as the third dimension, an approach similar to that of Hutchinson and Bischof (1983) is used in the RST module in GRASS; the interpolated function is therefore a function of horizontal co-ordinate as well as elevation. This can be interpreted as the intersection of the RST volume model of rainfall with the terrain surface (Neteler and Mitasova, 2002). The introduction of elevation as a co-variate serves as an important proxy for rainfall in complex data-sparse regions. Incorporating elevation in the interpolation tends to improve the results of interpolation (Goovaerts, 2000; Hofierka *et al.*, 2002).

This trivariate (3D, with elevation as the third dimension) form of RST method is implemented in the GRASS GIS as the module **v.vol.rst** (Neteler and Mitasova, 2002; GRASS, 2006). It requires the location and height of the rain gauges as the input to interpolate rainfall to a 3D grid. The resulting 2D rainfall field is obtained by intersecting the interpolated volume by the terrain surface represented by a DEM. An important feature of the implementation is a set of tuning parameters, which provide the flexibility needed in the interpolation procedure to represent the modelled phenomena. The most important parameters are tension (T) and smoothing (S) (Neteler and Mitasova, 2002). T controls the range over which a given point influences the resulting surface. For high T , each point influences only its close neighbourhood and the surface changes rapidly to the trend between the points. In 2D analogy, T tunes the interpolation surface from a stiff plate to an elastic membrane (Neteler and Mitasova, 2002). On the other hand, S allows the surface to deviate from the data points in an effort to minimize its energy. Low (high) S implies that the interpolation function passes close to (deviates more from) the data points. S is important when

using low T because it prevents overshoots (unusually high or low values); S also removes noise that may be present in the data (Neteler and Mitasova, 2002).

The optimal values of these parameters were chosen by minimization of the predictive error estimated by a Cross-Validation (CV) procedure (Tomczak 1988; Neteler and Mitasova, 2002), which is also incorporated in the *v.vol.rst* module (GRASS, 2006). In this approach, one data point was eliminated at a time, and the interpolation was performed using the remaining points. Then the residual between the actual value of the eliminated point and the value estimated (interpolated) at this point was computed. This procedure was repeated subsequently for all the data points. This resulted in the same number of residuals as the input data points. Then the overall performance of the interpolation was evaluated as the root mean of squared residuals (Root Mean Square Error, RMSE). This step was repeated for a range of values of T and S (0.01–0.09) and the combination that yielded the lowest RMSE was chosen as the optimal set of interpolation parameters. The entire procedure was carried out for the larger of the two domains shown in the map in Figure 1. The locations and heights were specified based on the GLOBE DEM grid, but these values were almost the same as the in-situ locations and heights given by IMD. (The averaging over a grid cell in the DEM implies that the height at a location in the DEM will not be equal to the IMD height in a region with complex terrain. The GLOBE values were preferred to the in-situ values for interpolation because the rainfall in any cell represents an average over the cell and is therefore not the same as the in-situ measurement using a rain gauge.)

The CV method provides an objective criterion to evaluate the selection of the interpolation parameters. Although there are many issues involved with the CV procedure, the final assessment of the spatial estimate of precipitation and its consistency should be judged by the discharge simulations, which provide an independent spatial climate element (Daly, 2006).

4. APPLICATION TO THE MANDOVI BASIN

4.1 Rainfall interpolation over the basin

We first interpolated the rainfall for 1981–1998 using the rain gauge data from 20 stations in and around the Mandovi basin (Figure 1). Of the 20 stations, data for only six (Castle Rock, Mormugao, Panaji, Sanguem, Khanapur, Kalasai, and Kumbarwada) were available over the entire analysis period (Table III). All available data, however, were used for interpolation in order to generate the best possible map for each month. The entire region (15° N–15° 48'N and 73° 36'E –74° 34'E) in the GLOBE DEM was divided into 96 X 116 grid cells with a resolution of 30 arc seconds. The T and S were varied in the range 0.01–0.09 to obtain optimal parameters by minimising the RMSE obtained through the CV procedure; the range for T and S was arrived at subjectively after a few interpolations. The RMSE for the optimum T and S (Figure 4) varied between 5.01 and 92.3 cm during the peak rainfall months (June–September). The resulting

rainfall maps were unable to capture the large gradients expected in the vicinity of the Sahyadris (Figure 5) owing to the poor rain-gauge coverage in the regions with large rainfall gradients, the ridge and the slopes of the Sahyadris. This poor coverage resulted in undershoots (low values) and overshoots (high values) when we tried to simulate the large rainfall gradient by reducing the smoothness of the rainfall surface (by lowering S). Hence, smoother surfaces had to be fitted to the rain-gauge data, resulting in the inability to simulate the large spatial gradients. When these rainfall maps were used to force THMB, the error in the simulated discharge at Ganjem, though now less than when the IMD data were used, was still too large (~14–44%) (Figure 5, Table II).

4.2 Separate interpolation for windward and leeward sides

The reason for the large errors in interpolation is the sparse distribution of rain gauges. This poor spatial sampling did not permit a clear separation between the windward and leeward sides, which is obvious in the large-scale rainfall distribution, to emerge naturally from the data. Hence, in order to overcome this problem, we interpolated the rainfall separately for the windward and leeward sides. We defined a ridge separating the windward and leeward sides, choosing, as a first approximation, the location of maximum elevation along a latitude circle as the ridge. This ridge was then subjectively edited where river valleys (like the Mandovi; see Figure 1) cut through the Sahyadris. This subjective editing was necessary to ensure a “reasonably” smooth and continuous ridge. This definition separated the domain into a high-rainfall windward side and a low-rainfall leeward side, with 10 rain-gauge stations on both sides (Table III). We then used the CV procedure to map the rainfall separately for each side; on both sides, the optimal T and S ranged between 0.01 and 0.09. The two maps were then merged using a 3-point smoothing:

$$R_i = (R_{i-1} + R_i + R_{i+1}) / 3 ,$$

where R_i is the rainfall in the first grid cell on the leeward side, R_{i+1} the (adjacent) leeward cell to its east and R_{i-1} the (adjacent) windward cell to its west; here, i is the zonal index. This smoothing was done (for each latitude) to ensure a smoother transition from the high rainfall on the windward side to the low rainfall on the leeward side.

The RMSE for the windward (leeward) side was 0–37.8 (0–94.2) cm (Figure 4). The reason for the larger error on the leeward side could not be ascertained, but we suspect the complex relation between rainfall and elevation and the clustering of rain gauges into two groups on the leeward side (Figure 1). The errors were, however, lower when the windward and leeward sides were mapped separately; note also that the leeward side constitutes a much smaller fraction of the catchment of the Mandovi at Ganjem, (~21% by area and on the average 13.8–20.4% by rainfall; see Table II). The RMSE values still seem large, but they are unavoidable in a data-sparse region like this: we have no means to compare the RMSE with any other studies in the region. The CV method also usually overestimates the interpolation error because the estimate is being computed at a location where data are genuinely available, and lack of data points aggravates this further (Hofierka *et al.* 2005).

The interpolated rainfall compared well with observed rainfall at the rain-gauge stations in the basin and at Castle Rock, the station nearest the ridge (but outside the Mandovi basin) (Figure 1 and Figure 6). The interpolation procedure captured the sharp increase in rainfall on the slopes (see panel for Gavali), but the rainfall was consistently underestimated on the windward side. On the leeward side (see panel for Asoga), the rainfall was consistently overestimated. This error was due to the curve tending to become smooth (in order to avoid overshoots) in regions that are data-sparse but have large gradients. The resulting rainfall maps were nevertheless able to catch the sharp increase in rainfall on the slopes of the Sahyadris, with the rainfall maximum hugging the Sahyadris (Figure 5). For the peak rainfall months, we obtained similar maps for all the years. THMB was then forced with the new rainfall maps. The simulated discharge compared well with the observed discharge at Ganjem (Figure 7 and Table IV). The error in simulated discharge was within the natural variability in the system (except in 1984 and 1988). The annual discharge error was less than 16% for 16 of 18 years; the average error over the 18 years was 8%. This is comparable to the measurement errors involved with discharge observations, which is of the order of ~15% (Dickinson, 1967; Cogley, 1989; Coe, 2000). Except in two years, the simulated discharge was lower than observed. This was due to the underestimation of rainfall at Gavali and Valpoi, which is representative of the heavy rainfall of the hill slopes. The percentage error was higher at Valpoi (often greater than 20%), but the much higher mean rainfall at Gavali implied that the smaller percentage error there led to a higher absolute rainfall error. Rain-gauge data for Gavali (Valpoi) were not available for 1984 (1988); these were the two years in which the discharge error (underestimate) exceeded 20% (Table II). The larger simulation errors occur in years when data for Gavali or Valpoi are missing (Table III and Table IV). The large error in 1998 is owing to data for six of the 10 windward stations have not being available. Note, however, that (as may be expected with the CV procedure) the RMSE is the error in rainfall at a station (Figure 6) and bears no obvious relation to the error in simulated discharge (Table IV and Figure 7).

The simulated discharge showed larger errors when compared with the discharge measurements at Kulem on the Khandepar (Figure 7, Table IV). One reason for this larger simulation error is the much lower discharge of the Khandepar. Another reason is the absence of critical data. The discharge errors are largest (greater than 25%) during 1983–1985, when the observed discharge was high and rainfall data for Gavali were missing. (Note that data for several stations were missing in 1998, another year with a large error.) There are no rain-gauge stations on the slopes in the Khandepar basin, implying a high impact of Gavali and Castle-Rock rainfall on the discharge simulated at Kulem. Absence of data at Gavali therefore leads to an underestimate in basin rainfall, the error being larger when the rainfall is high because the highest rainfall (and the highest standard deviation) is on the slopes of the Sahyadris (Table 3). Note, however, that the discharge during 1983–1985 at Ganjem was closer to the mean discharge, suggesting an unmapped, higher-than-normal rainfall in the Khandepar basin. Since the available data do not suggest a north–south trend during these years, it is likely that the excess rainfall in the Khandepar basin was restricted to it. The absence of a rain gauge in the basin makes it impossible to resolve the spatial variation any better than done above. Hence, the method is only as good as is the

distribution of data: sparsity of data implies larger errors in smaller sub-basins.

Nevertheless, the mean simulated discharge was lower at both Ganjem and Kulem. The simulated variance was also lower than the observed variance. Both point to a smoother rainfall map than probably exists in nature, with the sparse coverage of the basin, especially on the hill slopes, resulting in a lower estimate of basin rainfall than observed. A consequence of this sparse coverage is the lack of variation in rainfall between Gavali and Castle Rock, which are separated by ~25 km (Figure 1). Though Gavali is at a higher elevation (Table III), Castle Rock is on the ridge and Gavali on the slopes. The observed rainfall is higher at Gavali than at Castle Rock, but the sparsity of rain gauges masks this spatial gradient. Data from south of Goa also show that, in accordance with theory (Sarker, 1967), the maximum rainfall occurs on the windward slope of the Sahyadris (Gavali, for example), not on the ridge (Castle Rock, for example) (Basappa and Jose, 2007). Hence, sparsity of data, which is common in the vicinity of the Sahyadris, will imply a similar rainfall underestimate all along the Indian west coast.

The results did not show an obvious relationship between the rainfall RMSE and the discharge errors: the correlation between the two errors is low. It is known, however, that the CV method does not provide optimum parameters in all cases, and it is dependent on the density and homogeneity of data points (Hofierka *et al.* 2005; Daly 2006). The THMB simulations were able to capture the variability in discharge observations reasonably well on the annual scale (Table IV, Figure 7), and since the discharge is an independent measure of the rainfall interpolation, it is a more stringent test of the rainfall interpolation (Daly, 2006).

4.3 Sensitivity to evapo-transpiration estimates

Apart from the uncertainty associated with the rainfall, there is the uncertainty associated with the evapo-transpiration field, which is part of the forcing for THMB. We used the NCEP/NCAR Reanalysis (Kalnay *et al.*, 1996) for evapo-transpiration estimates. Large positive biases in these estimates have been reported from the Mississippi basin (Roads and Betts, 1999). Though this study is from the extra-tropics, it is evident that a class C variable like evapo-transpiration is prone to errors (Kalnay *et al.*, 1996). The evapo-transpiration does not affect the discharge to the lowest order because it is a couple of orders of magnitude smaller (for the annual total) than the rainfall on the Indian west coast (Shankar *et al.*, 2004). We therefore tested the sensitivity of our results to a one standard-deviation (~5–14%, with the lower end of the range applicable to the high-rainfall summer-monsoon months) change in evapo-transpiration. There was a little improvement for the years with a negative discharge error when the evapo-transpiration was reduced, but the discharge error for 1984 and 1988 was still greater than 20%. Decreasing evapo-transpiration (uniformly in time) by 20%, the value given by Roads and Betts (1999), for each month reduced the discharge error for 1984 (1988) from 21.1% (22.4%) to 17.8% (19.96%).

5. DISCUSSION

We have shown that an interpolation algorithm that includes elevation as a co-variate yields a better rainfall map for the Mandovi basin than an algorithm that ignores elevation. This is owing to the influence of orography on the rainfall on the Indian west coast. The IMD interpolation, which did not account for elevation, also excluded several stations that did not have a long record in order to produce a consistent estimate of the rainfall. Hence, the interpolated IMD rainfall underestimated the rainfall over the Mandovi basin. A key result is that in data-sparse regions with a complex mountainous terrain (like the Mandovi basin), it is better to extract the ridge line *a priori* and map the windward and leeward sides separately. This separate mapping reduces the underestimation of rainfall by ensuring that the sharp decline in rainfall across the ridge, which does not emerge naturally from a combined mapping of the entire basin, is now guaranteed to the extent that rain-gauge data are available on the slopes and the ridge. Note that such subjectivity is common in geostatistical techniques like kriging.

The resolution of the interpolation also matters. The CRU data set also includes elevation as a co-variate, but the 0.5° resolution of the data set was too crude for it to resolve the sharp rainfall gradient induced by the Sahyadris. Interpolating the rainfall at a high resolution and then downscaling the interpolated rainfall to a coarser grid also proved superior to an interpolation at a coarse resolution. We downscaled the rainfall interpolated at 30 arc seconds to a 0.25° grid and then forced THMB (at a 30-arc-seconds resolution) with the resulting rainfall map. The rainfall forcing, as with the TRMM/CRU/IMD data sets, was now invariant over the larger 0.25° grid, but the results were superior to those obtained with the other data sets: the average discharge error was 4.8% (underestimate), as opposed to 8% when THMB was forced with the interpolated rainfall at 30 arc seconds resolution without any rescaling (Table IV). (The lower error does not imply that rescaling is better. For the Mandovi basin, the positioning of the low-resolution and high-resolution grids means higher rainfall from outside the basin 'spilled' into the basin, resulting in a positive rainfall error that countered the overall underestimation of basin rainfall.) When the terrain is complex and data are sparse, it is important to grid the rainfall at a high resolution even if the final resolution at which data are required is much lower. Hence, if hydrological consistency is an objective, mapping at different resolutions in different regions may be necessary, the maps being subsequently rescaled to the common desired resolution. In other words, the IMD data set (Rajeevan *et al.*, 2006a,b) might have benefited from a higher resolution of the mapping grid along the Indian west coast; the coarser grid is probably sufficient in the low-gradient terrain common over most of India. The final data set could always be prepared at a common resolution by downscaling the high-resolution maps to the best common resolution possible.

As stated in the introduction, the main motivation for this work lies in the need to estimate the discharge into the seas around India. Ganjem, where the discharge gauge on the Mandovi is located, is 50 km upstream, making it an unsuitable measure of the discharge at Panaji, which is at the mouth. An estimate for the Mandovi's discharge was reported by Rao (1975). The Ganjem gauge did not exist then and Rao used a classification and extrapolation scheme to estimate the

discharge. Based on data for gauged rivers in India, Rao (1975) estimated that the discharge for river basins with “high” rainfall was of the order of 65 Mm³ per 100 sq. km. of basin area. This method yielded a value of ~1320 Mm³ for the Mandovi. Which is almost a third of the discharge measured at Ganjem. This result is not surprising because the data used by Rao were from rivers spread across India, and rainfall varies from over 600 cm to less than 20 cm over the country. Our estimate of the discharge at Panaji (Table IV) was over 6004 Mm³, with a standard deviation of 890 Mm³. The ratio of the discharge at Panaji to that at Ganjem varied between 1.8–2.1 for the simulated discharge. Since the variance of the simulated discharge at Ganjem was lower than that of the observed discharge, the simulated variance at Panaji is also likely to be lower than in reality. Nevertheless, the lower error in interpolated rainfall at the coastal stations compared to the stations on the hill slopes (compare Panaji with Gavali in Figure 6) implies that the percentage error at Ganjem can be considered an upper bound on the percentage error at Panaji. The climatological discharge estimated by Fekete *et al.* (2000) for this part of the Indian west coast compares favourably with ours, but the former is at the much coarser resolution of 0.5°. Since the Mandovi is typical of the rivers along the Indian west coast, the method outlined here is extensible to the rest of the coast.

The results presented here are significant because an independent measure, the discharge, has been used to validate the rainfall interpolation algorithm. The interpolated monthly rainfall, when used to force THMB, produced an annual discharge estimate within 15–20% of the observations. Simulations forced with interpolated annual rainfall, however, resulted in larger errors: though the interpolation error was lower for annual rainfall, the discharge error was higher because the annual-rainfall map was much smoother and underestimated the rainfall over the Sahyadris. This implies that the objective of simulating the monthly discharge will require the rainfall interpolation to be done on shorter time scales. The sparsity of rain gauges is likely to result in larger mapping errors in this case, but the discharge error may still be less than the error in monthly discharge when monthly rainfall maps are used as the forcing.

Simulating the monthly discharge of the Mandovi will also present another challenge. The seasonality of rainfall over the Indian west coast, with there being almost no rain during January–April, implies that each year's result is independent of that of the preceding years: the system has no memory as far as annual discharge is concerned and there is no correlation between the discharge of two successive years. Physically, the land dries up soon after the rains cease, and the next year's rains fall on empty surface and sub-surface reservoirs. Hence, the annual discharge curve starts at almost zero each year (and is almost zero till April). Therefore, the integral of monthly discharge for each year is independent of the details of the discharge curve and is a function of only the total rainfall over (and evapo-transpiration from) the basin. Hence, the details of model parameterisation were not important for simulating the annual discharge: the residence times of the surface (T_s) and sub-surface (T_d) reservoirs and the partitioning of local runoff between surface and sub-surface runoff could be held constant (as in the simulations of Coe (2000) and Shankar *et al* (2004)) without it affecting the result.

With monthly discharge, however, this will no longer hold, the time scales now being short enough for the sub-surface reservoir to retain information from the previous month. In the simulations reported here, the monthly discharge was considerably underestimated during the peak monsoon months of July and August and overestimated before (May–June) and after the monsoon peak (September–December). Hence, for simulating monthly discharge, two changes will be needed: the residence time of the sub-surface reservoir (T_d) and the partitioning between the surface and sub-surface runoff will have to be made functions of time. The method outlined above for mapping monthly rainfall should, however, be applicable for daily rainfall.

ACKNOWLEDGEMENTS

This work was supported by grants from the Department of Ocean Development, India. Suprit Kumar acknowledges the financial support from Council of Scientific and Industrial Research, India. S.R. Shetye inspired and encouraged us to take up this work. IMD and CWC provided the rainfall and river-discharge data; M. Rajeevan and O.P. Sreejith of IMD helped with the rainfall data and answered many questions concerning them. Helena Mitsova answered our queries on the RST method. We acknowledge the helpful discussions we had with V. Venugopal and D. Nagesh Kumar, Indian Institute of Science. We acknowledge the role of GRASS GIS in this study and thank the GRASS team. The comments of Michael Coe and an anonymous reviewer helped improve the manuscript; in particular, they pointed out that the key result of this study, separate mapping for windward and leeward sides, needed highlighting. Nagesh Bhatkar ported the DEM editing software of Kotamraju and Shankar (2004) to GRASS 6.0. Ferret and GMT were also used extensively for analysis and graphics. We thank A.Y. Mahale for helping with the figures. This is NIO contribution 4237.

REFERENCES

- Basappa V, Jose MK. 2007. Identification of homogeneous rainfall regimes in parts of Western Ghats region of Karnataka. *Journal of Earth System Science* **116**: (In press)
- Coe MT. 1998. A linked global model of terrestrial hydrologic processes: Simulation of modern rivers, lakes and wetlands. *Journal of Geophysical Research* **103**: 8885–8899.
- Coe MT. 2000. Modeling terrestrial hydrological systems at the continental scale: Testing the accuracy of an atmospheric GCM. *Journal of Climate* **13**: 686–704.
- Cogley JG. 1989. Run-off from the world's landmasses: Amounts and uncertainties at 2-degree resolution. Trent Climate Note 89-3, p. 25.
- Cressie NAC. 1993. Statistics for spatial data. John Wiley & Sons Inc, New York.
- Daly C. 2006. Guidelines for assessing the suitability of spatial climate data sets. *International Journal of Climatology* **26**: 707–721
- Dickinson WT. 1967. Accuracy of discharge determinations. Hydrology Paper 20, Colorado State University, Fort Collins, CO 80523, USA.
- ETOPO2. 2007. On-line documentation. <http://www.ngdc.noaa.gov/mgg/fliers/06mgg01.html>. [Last accessed 14 January 2007]
- Fekete BM, Vorosmarty CJ, Grabs W. 2000. Global composite runoff fields on observed river discharge and simulated water balances. Report 22. Global Runoff Data Centre, Koblenz, Germany.
- Frei C, Schar C. 1998. A precipitation climatology of the Alps from high resolution rain-gauge observations. *International Journal of climatology* **18**: 873–900.
- Goovaerts P. 2000. Geostatistical approaches for incorporating elevation into the spatial interpolation of rainfall. *Journal of Hydrology* **228**: 113–129.
- GLOBE. 2004. The Global Land One kilometer Base Elevation (GLOBE) Digital Elevation Model. Version 1.0. National Oceanic and Atmospheric Administration, National Geophysical Data Center, <http://www.ngdc.noaa.gov/mgg/topo/globe.html>. [Last accessed 12 January 2007]
- Graham ST, Famiglietti JS, Maidment DR. 1999. 5-minute, 0.5-degree, and 1-degree data sets of continental watersheds and river networks for use in regional and global hydrologic and climate

system modeling studies. *Water Resources Research* **35**: 583–587.

GRASS Development Team. 2006. Geographic Resources Analysis Support System (GRASS) Software. ITC-irst, Trento, Italy. <http://grass.itc.it> [Last accessed 12 January 2007]

Han W, McCreary JP, Kohler KE. 2001. Influence of precipitation minus evaporation and Bay of Bengal rivers on dynamics, thermodynamics, and mixed layer physics in the upper Indian Ocean. *Journal of Geophysical Research* **106**: 6895–6916.

Han W, Webster PJ. 2002. Forcing mechanism of sea level interannual variability in the bay of Bengal. *Journal of Physical Oceanography* **32**: 216–239

Hofierka J, Parajka J, Mitasova H, Mitas L. 2002. Multivariate interpolation of precipitation using regularized spline with tension. *Transactions in GIS* **6**: 135–150.

Hofierka J, Cebecauer T, Šúri M. 2005. Optimisation of interpolation parameters using a cross-validation. Submitted to: Peckham R., Jordan G. (eds.) Best Practice in Digital Terrain Modelling: Development and Applications in a Policy Support Environment. European Commission Joint Research Centre, Ispra (VA).

Howden SD, Murtugudde R. 2001. Effect of river inputs into the Bay of Bengal. *Journal of Geophysical Research* **106**: 19825–19843.

Hutchinson MF, Bischof RJ. 1983. A new method for estimating the spatial distribution of mean seasonal and annual rainfall applied to Hunter Valley, New South Wales. *Australian Meteorological Magazine* **31**: 179–184.

Hutchinson MF. 1995. Interpolation of mean rainfall using thin plate smoothing splines. *International Journal of Geographical Information Systems* **9**: 385–403.

Hutchinson MF. 1998a. Interpolation of rainfall data with thin plate smoothing splines - Part I: Two dimensional smoothing of data with short range correlation. *Journal of Geographic Information and Decision Analysis* **2**:139–151.

Hutchinson MF. 1998b. Interpolation of rainfall data with thin plate smoothing splines - Part II: Analysis of topographic dependence. *Journal of Geographic Information and Decision Analysis*, **2**: 152–168.

Janowiak JE, Gruber A, Kondragunta CR, Livezey RE, Huffman GJ. 1998. A comparison of the NCEP–NCAR reanalysis precipitation and the GPCP rain-gauge–satellite combined data set with observational error considerations. *Journal of Climate* **6**: 1009–1026

Jeffrey JS, Carter JO, Moodie KB, Beswick AR. 2001. Using spatial interpolation to construct a comprehensive archive of Australian climate data, *Environmental Modeling & Software* **16**: 309–330.

Journel AG. 1996. Modelling uncertainty and spatial dependence: stochastic imaging. *International journal of Geographical Information Systems* **10**: 517–22

Kalnay, E, Kanamitsu M, Kistler R, Collins W, Deaven D, Gandin L, Iredell M, Saha S, White G, Woollen J, Zhu Y, Chelliah M, Ebisuzaki W, Higgins W, Janowiak J, Mo KC, Ropelewski C, Wang J, Leetmaa A, Reynolds R, Jenne R, Joseph D. 1996. The NCEP/NCAR 40-year reanalysis project. *Bulletin of the American Meteorological Society* **77**: 437–471.

Kotamraju V, Shankar D. 2004. Using the GRASS GIS in a framework for quantifying water resources in India. Poster presented at MapIndia 2004, New Delhi, India.

Martin JM, Barton JD, Eisma D. 1981. River inputs to ocean systems. United Nations Press, New York.

Mitas L, Mitasova H. 1999. Spatial Interpolation. In: Geographical Information Systems, Vol. 1, Principles and technical issues, second edition. Longley PA, Goodchild MF, Maguire DJ, Rhind DW. (Eds.). John Wiley & Sons: 481-492.

Mitasova H, Mitas L. 1993. Interpolation by regularized spline with tension: I. Theory and implementation. *Mathematical Geology* **25**: 641–655.

New MG, Hulme M, Jones PD. 1999. Representing twentieth-century space–time climate variability. Part I: Development of a 1961–90 mean monthly terrestrial climatology. *Journal of Climate* **12**: 829–856.

New MG, Hulme M, Jones PD. 2000: Representing twentieth-century space–time climate variability. Part II: Development of 1961–90 monthly grids of terrestrial surface climate. *Journal of Climate* **13**: 2217–2238.

Neteler M. Mitasova H. 2002. Open Source GIS: A GRASS GIS Approach. Kluwer Academic Publishers: Dordrecht, The Netherlands.

Rajeevan M, Bhate J, Kale JD, Lal B. 2006a. Development of a high resolution daily gridded rainfall data set for the Indian region. IMD Meteorological Monograph No. Climatology 22/2005. India Meteorological Department, Pune, India.

Rajeevan M, Bhate J, Kale JD, Lal B. 2006b. High resolution daily gridded rainfall data for the Indian region: Analysis of break and active monsoon spells. *Current Science* **86** (3): 296–306.

- Rao KN, Raman CRV, Daniel CEJ, Venkataraman S. 1971. Evaporation over India. Technical Report PPSR No. 146, India Meteorological Department, Meteorological Office, Pune, India.
- Rao KL. 1975. *India's Water Wealth: Its assessment, uses and projections*. Orient Longman: New Delhi.
- Roads J, Betts A. 1999. NCEP-NCAR and ECMWF Reanalysis surface water and energy budget for the Mississippi river basin. *Journal of Hydrometeorology* **1**: 88-94
- Sarker RP. 1966. A dynamical model of orographic rainfall. *Monthly Weather Review* **94**: 555-572.
- Sarker RP. 1967. Some modifications in a dynamical model of orographic rainfall. *Monthly Weather Review* **95**: 673-684.
- Shankar D. 2000. Seasonal cycle of sea level and currents along the coast of India. *Current Science* **78**: 279-288.
- Shankar D, Shetye SR. 1999. Are interdecadal sea level changes along the Indian coast influenced by variability of monsoon rainfall? *Journal of Geophysical Research* **104**: 26031-26042.
- Shankar D, Shetye SR. 2001. Why is mean sea level along the Indian coast higher in the Bay of Bengal than the Arabian Sea? *Geophysical Research Letter* **28**; 563-565.
- Shankar D, Kotamraju V, Shetye SR. 2004. A quantitative framework for estimating water resources in India. *Current Science* **86**: 543-552.
- Shankar D, Shenoi SSC, Nayak RK, Vinayachandran PN, Nampoothiri G, Almeida AM, Michael GS, Rameshkumar MR, Sundar D, Sreejith OP. 2005. Hydrography of the eastern Arabian Sea during summer monsoon 2002. *Journal of Earth System Science* **114**: 459-474.
- Shenoi SSC, Shankar D, Shetye SR. 2002. Differences in heat budgets of the near-surface Arabian Sea and Bay of Bengal: Implications for the summer monsoon. *Journal of Geophysical Research* **107**: 10.1029/2000JC000679.
- Shetye SR, Gouveia AD, Singbal SY, Naik CG, Sundar D, Michael GS, Nampoothiri G. 1995. Propagation of tides in the Mandovi-Zuari estuarine network. *Proceedings of Indian Academy of Sciences. (Earth Planetary Sciences)* **104**: 667-682.
- Suprit K, Shankar D. 2006. Simulating the discharge of the Mandovi River, Goa. Prediction in ungauged basins for sustainable water resources planning and management. Raju KS (Ed.). Jain

Brothers, New Delhi: 175–186

Tomczak M. 1988. Spatial interpolation and its uncertainty using automated anisotropic inverse distance weighting (IDW): Cross-validation/jackknife approach. *Journal of Geographical Information and Decision Analysis* **2**: 18–33.

TRMM. 2006. On-line documentation. <http://trmm.gsfc.nasa.gov/3b43.html> [Last accessed on 12 January 2007]

USGS. 2004. Shuttle Radar Topography Mission (SRTM), 3 Arc Second scene, Unfilled Unfinished 2.0. Global Land Cover Facility, University of Maryland, College Park, Maryland. (<http://glcf.umiacs.umd.edu/data/srtm/>). [Last accessed on 27 February 2007]

Vörösmarty CJ, Fekete BM, Tucker BA. 1996. Global river discharge database (RivDis Version 1.0), Vol. 0: Introduction, overview, and technical notes. International Hydrological Program Technical; Document in Hydrology SC. 96/WS/26. UNESCO, Division of Water Sciences, 1 rue Miollis, 75732 Paris, France.

Xie S-P, Xu H, Saji NH, Wang Y, Liu WT. 2006. Role of narrow mountains in large-scale organization of Asian monsoon convection. *Journal of Climate* **19**: 3420–3429

Yaremchuk M, Yu Z, McCreary JP. 2005. River discharge into the Bay of Bengal in an inverse ocean model. *Geophysical Research Letters* **32**: 10.1029/2005GL023750.

List of Tables

Table I. Description of the gridded rainfall data sets used in this study.

Table II. Comparison of simulated and observed discharges at Ganjem; all the discharges are in 10^6 m^3 or Mm^3 . Column 2 (C2): Observed discharge at Ganjem (O_G); C3: simulated discharge at Ganjem for CRU forcing; C4: as in C3, but for IMD forcing; C5: as in C3, but for forcing with interpolated (windward and leeward sides combined) rainfall (S_C is the simulated discharge for this experiment); and C6: as in C5, but with the rainfall interpolation done separately for the windward and leeward sides (S_{WL} is the simulated discharge for this experiment). In columns 3–6, the numbers in parenthesis denote percentage error (simulated minus observed discharge). Columns 7 (P_W) and 8 (P_L) are the areal rainfall in Mm^3 over the windward and leeward parts, respectively, over the catchment area at Ganjem for the forcing used in S_{WL} . The last two rows of table show the mean (percentage error in parentheses) and standard deviation (SD) of the respective variables.

Table III. Name, location (latitude (longitude) in degrees north (east)) and height (m) of the rain-gauge stations used in this study, along with a summary of the annual rainfall statistics (mean and SD; cm/year). Stations in the top (bottom) half of the table are from the windward (leeward) side of the Sahyadris. Column 5 lists the years for which data were not available (at least for the monsoon months).

Table IV. Results of the simulations and sensitivity experiments; all the discharges are in 10^6 m^3 or Mm^3 . Column 2 (C2): Observed discharge at Ganjem (O_G); C3: simulated discharge (S_{WL} ; see Table II) at Ganjem; C4 ($S_G + 1E$): discharge at Ganjem for a one-SD (standard deviation) increase in evapo-transpiration; C5 ($S_G - 1E$): discharge at Ganjem for a one-SD decrease in evapo-transpiration; C6: observed discharge at Kulem (O_K); C7: simulated discharge at Kulem (S_K); and C8: simulated discharge at Panaji (S_P). In columns 3–5 and 7, the numbers in parentheses denote percentage error (simulated minus observed) with respect to the observed discharges. Column 9 shows the difference between the discharge at Panaji and the sum of the simulated discharges at Ganjem and of the Khandepar (estimated where it joins the Mandovi); this is therefore the contribution of the other, minor tributaries of the Mandovi downstream of where it meets the Khandepar and of the direct flow into the Mandovi estuary. Comparisons show that most of this inflow comes from the minor tributaries. The last two rows of table show the mean (percentage error, wherever applicable is shown in parenthesis) and standard deviation (SD) of the simulations. All the discharges are in 10^6 m^3 or Mm^3 .

List of Figures

Figure 1*. The region of interest. The topography of the region (along with 0 and 500m contours) as in the edited GLOBE DEM (inset topography from ETOPO2 (ETOPO2, 2007)). The Mandovi and Zuari (all rivers digitized from Survey of India maps) are the two major rivers of Goa (border overlaid on the map). The Mandovi originates in the Sahyadris and drains into the Arabian Sea near Panaji. The Mandovi basin (black curve) has two discharge gauging stations, at Ganjem on the Mandovi itself and at Kulem on its major tributary, the Khandepar. The outer and inner rectangles denote the interpolation and THMB model domains; rainfall interpolation was performed over a larger domain in order to include more rain gauges to map the variation. The region has two distinct topographical and climatic features: to the west lies a coastal plain with heavy rainfall (windward side), and to the east lies a plateau with less rainfall (leeward side). The white jagged line is the ridge separating the windward and leeward sides of the Sahyadris. Stations on the windward (leeward) sides are marked in black (white).

Figure 2. Influence of topography on rainfall. The topography (meridionally averaged over the interpolated domain) of region is shown shaded along with the mean monsoonal precipitation (for June–September) along an approximate east-west transect passing through Panaji and Khanapur (see Figure 1). The symbol at the top of the shaded topography marks the station location. The same symbol is used to denote the rainfall at that station. For example, the lower (upper) asterisk (inverted triangle) for Panaji (Asoga) marks the location and the upper (lower) asterisk (inverted triangle) the rainfall at Panaji (Asoga) Note that the heights shown are not the station heights but the meridional average of the elevation at a given distance from the coast. All the stations shown, except Ponda and Khanapur, lie in the Mandovi basin.

Figure 3*. Rainfall distribution in July for the CRU, IMD, and TRMM data sets. The upper left panel shows the two discharge gauging stations. Note the different spatial resolutions of these gridded data sets. See the text for an explanation for the “W” and “E” marked on the panel for the IMD data set and the solid dot marked on the panel for the CRU data set.

Figure 4. RMS error (RMSE, in cm) for obtaining optimal tension and smoothing parameters to be used in rainfall interpolation. The top panel shows the RMSE when interpolation was done for windward and leeward stations combined (discharge S_C in Table II); the bottom panel shows the RMSE for separate interpolation for windward and leeward sides (discharge S_{WL} in Table II).

Figure 5*. Interpolated rainfall maps for August 1982. The left (right) panel is for simulation S_C (S_{WL}). The black curve is the Mandovi basin. The ridge separating the windward and leeward sides is shown by the grey curve in the right panel. The six rain-gauge stations (1–6) are the ones for which estimated and observed rainfall are compared in Figure 6.

Figure 6. Interpolated and observed rainfall (in cm/year) at the stations marked in Figure 5; note that Castle Rock is not in the Mandovi basin, but is the only station on the ridge for which data

were available. The vertical bars are a measure of the variability in the observed rainfall; the length represents one standard deviation on either side of the observed rainfall.

Figure 7. Simulated discharges at Ganjem and Panaji (top panel) and Kulem (bottom panel). The observed discharge is plotted for comparison. The shaded area is a measure of the variability in the observed discharge; the shading is done for one standard deviation on either side of the observed discharge. The black curve is the simulated discharge. Note the negligible impact of evapo-transpiration (indicated by the thickness of the black curve) and that the error in simulated discharge is within the natural variability of the system (except in 1984 and 1988, where the black curve falls just outside the shaded region).

- **(Note):** Figures 1, 3 and 5 are provided as colour illustrations for the on-line PDF version. The print version of these figures will not be in colour.

Table I.

Datasets	Resolution	Type	Remarks
NCEP/NCAR	2.5°, Monthly, Global	Model Reanalysis	(Shankar <i>et al.</i> 2004)
CRU TS 2.0	0.5°, Monthly, Global	High resolution gridded observed dataset	Available from CRU, Uni. of East Anglia; http://www.cru.uea.ac.uk/~timm/grid/CRU_TS_2_0.html
IMD	1.0°, Daily, Regional	—do —	Available from IMD; (Rajeevan <i>et al.</i> 2006a,b)
TRMM	0.25°, Monthly, Tropics	Merged TRMM instruments and other	Algorithm 3B43; http://trmm.gsfc.nasa.gov/3b43.html

Table II.

<i>Year</i>	<i>O_G</i>	<i>CRU</i>	<i>IMD</i>	<i>S_C</i>	<i>S_{WL}</i>	<i>P_W</i>	<i>P_L</i>
1981	3895	2188 (-43.8)	2338 (-40.0)	3001 (-22.9)	3581 (-8.1)	3585	770
1982	4214	1456 (-65.4)	1943 (-53.9)	2522 (-40.2)	3554 (-15.7)	3631	757
1983	3787	2413 (-36.3)	2561 (-32.4)	2648 (-30.1)	3603 (-4.9)	3587	740
1984	3540	1329 (-62.5)	1523 (-57.0)	2003 (-43.4)	2793 (-21.1)	2887	634
1985	3171	1005 (-68.3)	2003 (-36.8)	2115 (-33.3)	2865 (-9.6)	2943	637
1986	2543	1214 (-52.3)	1068 (-58.0)	1678 (-34.0)	2490 (-2.1)	2620	555
1987	2275	866 (-61.9)	1700 (-25.3)	1768 (-22.3)	2246 (-1.3)	2531	404
1988	4187	2092 (-50.0)	1943 (-53.6)	2353 (-43.8)	3251 (-22.4)	3309	643
1989	2762	1302 (-52.9)	1633 (-40.9)	2102 (-23.9)	2921 (5.8)	2986	603
1990	4018	1230 (-69.4)	1748 (-56.5)	2552 (-36.5)	3713 (-7.6)	3823	804
1991	3305	1582 (-52.1)	1442 (-56.4)	2203 (-33.3)	3024 (-8.5)	3092	726
1992	3326	1849 (-44.4)	1661 (-50.1)	2346 (-29.5)	3109 (-6.5)	3189	714
1993	3333	1466 (-56.0)	1456 (-56.3)	2113 (-36.6)	2910 (-12.7)	3046	682
1994	4718	2545 (-46.1)	1734 (-63.2)	3140 (-33.4)	4177 (-11.5)	4021	1025
1995	2940	1036 (-64.8)	2298 (-21.8)	1964 (-33.2)	2534 (-13.8)	2806	542
1996	2557	1448 (-43.4)	2098 (-17.9)	2193 (-14.2)	2903 (13.5)	3026	620
1997	3721	2214 (-40.5)	2170 (-41.7)	2673 (-28.2)	3496 (-6.1)	3451	884
1998	2906	1658 (-42.9)	1870 (-35.7)	1877 (-35.4)	2440 (-16.0)	2686	559
Mean	3400	1605 (-53)	1844 (-44)	3075 (-32)	3031 (-8)	3179	683
SD	648	489	359	391	501		

Table III.

<i>Station</i>	<i>Longitude</i>	<i>Latitude</i>	<i>Height</i>	<i>Missing years</i>	<i>Mean</i>	<i>SD</i>
Castle Rock	74.35	15.4	559	—	597.8	93.1
Gavali	74.26	15.6	744	1982–85,1997	661.1	172.7
Madgaon	73.96	15.28	10	1988,1998	292.8	58.2
Mhapsa	73.8	15.59	22	1988–89,1998	303.1	57.6
Mormugao	73.79	15.41	22	—	270.9	39.9
Panaji	73.81	15.48	1	—	286.0	45.0
Ponda	74.02	15.4	32	1988,1998	332.0	61.6
Quepem	74.06	15.21	48	1987–89,1998	357.3	83.8
Sanguem	74.15	15.23	52	1998	361.7	50.3
Valpoi	74.13	15.55	67	1988,1993–95,1998	413.2	56.2
Asoga	74.36	15.6	692	1997	160.5	49.5
Desur	74.5	15.75	732	1985,1997	143.8	34.5
Jamagaon	74.48	15.55	673	1982,1984–85	394.0	96.7
Khanapur	74.51	15.63	646	—	183.0	42.8
Londa	74.5	15.45	650	1984–85,1987–89,1997	227.8	93.5
Akheti	74.42	15.75	766	1987	519.2	101.1
Jagalpet	74.5	15.25	515	1987,1998	256.2	61.2
Kalasai	74.42	15.07	640	—	327.3	59.3
Kumbarwada	74.46	15.14	614	—	366.9	100.1
Kundar	74.35	15.14	666	1989	498.8	121.7

Table IV.

<i>Year</i>	O_G	S_G		S_{G+1E}		S_{G-1E}	O_K	S_K		S_P	S_{P-} (S_G+S_{Kt})	
1981	3895	3581	(-8.1)	3551	(-8.8)	3612	(-7.3)	468	452	(-3.4)	7162	2009
1982	4214	3554	(-15.7)	3520	(-16.5)	3589	(-14.8)	543	464	(-14.5)	6979	1836
1983	3787	3603	(-4.9)	3573	(-5.6)	3633	(-4.1)	653	460	(-29.6)	7267	2043
1984	3540	2793	(-21.1)	2758	(-22.1)	2828	(-20.1)	645	375	(-41.9)	5390	1382
1985	3171	2865	(-9.6)	2832	(-10.7)	2897	(-8.6)	610	357	(-41.5)	5738	1583
1986	2543	2490	(-2.1)	2463	(-3.1)	2520	(-0.9)	450	353	(-21.6)	4627	1076
1987	2275	2246	(-1.3)	2213	(-2.7)	2279	(0.2)	343	298	(-13.3)	4621	1323
1988	4187	3251	(-22.4)	3221	(-23.1)	3280	(-21.7)	488	447	(-8.3)	6398	1704
1989	2762	2921	(5.8)	2893	(4.7)	2949	(6.8)	416	391	(-6.1)	5611	1423
1990	4018	3713	(-7.6)	3669	(-8.7)	3757	(-6.5)	623	534	(-14.3)	6857	1631
1991	3305	3024	(-8.5)	2999	(-9.3)	3050	(-7.7)	473	414	(-12.4)	5634	1354
1992	3326	3109	(-6.5)	3074	(-7.6)	3143	(-5.5)	441	409	(-7.3)	6042	1608
1993	3333	2910	(-12.7)	2875	(-13.7)	2945	(-11.6)	468	403	(-13.8)	5501	1348
1994	4718	4177	(-11.5)	4141	(-12.2)	4214	(-10.7)	622	593	(-4.8)	7472	1677
1995	2940	2534	(-13.8)	2498	(-15.0)	2569	(-12.6)	407	322	(-20.9)	5320	1614
1996	2557	2903	(13.5)	2868	(12.2)	2939	(14.9)	429	372	(-13.4)	5734	1540
1997	3721	3496	(-6.1)	3467	(-6.8)	3527	(-5.2)	526	440	(-16.4)	6844	1829
1998	2906	2440	(-16.0)	2404	(-17.3)	2476	(-14.8)	434	323	(-25.5)	4866	1357
Mean	3400	3031	(-8)	3057	(-9)	3123	(-7)	502	411	(-17)	6004	1574
SD	648	501		501		503		91	73		890	247

Figure 1

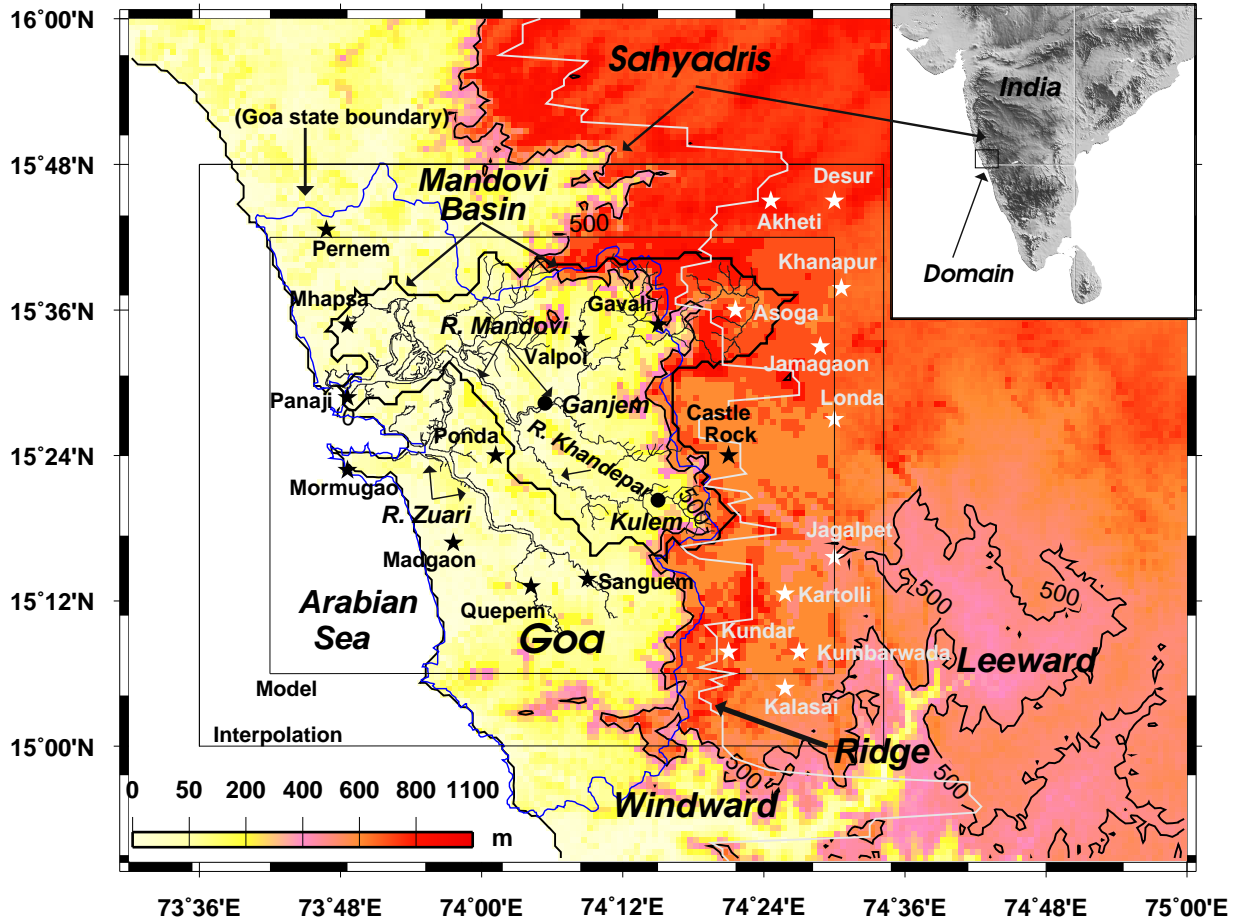


Figure 2

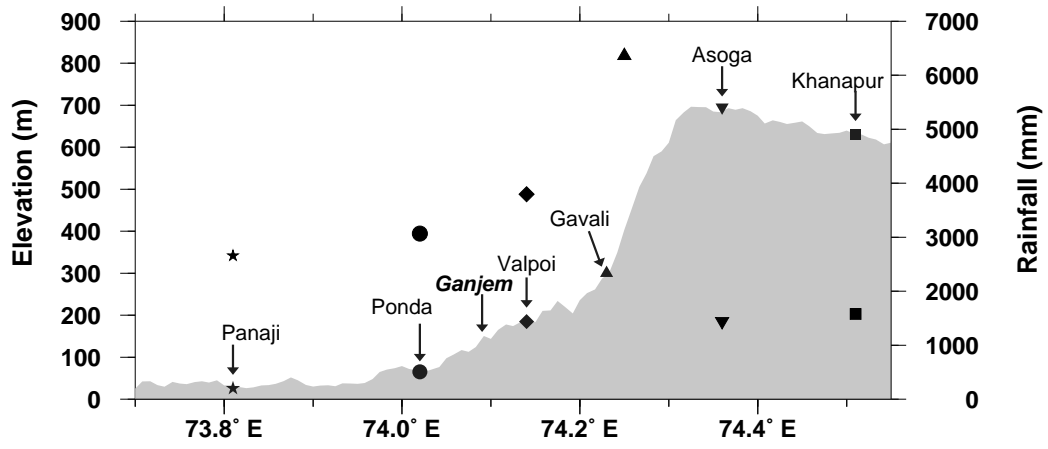


Figure 3

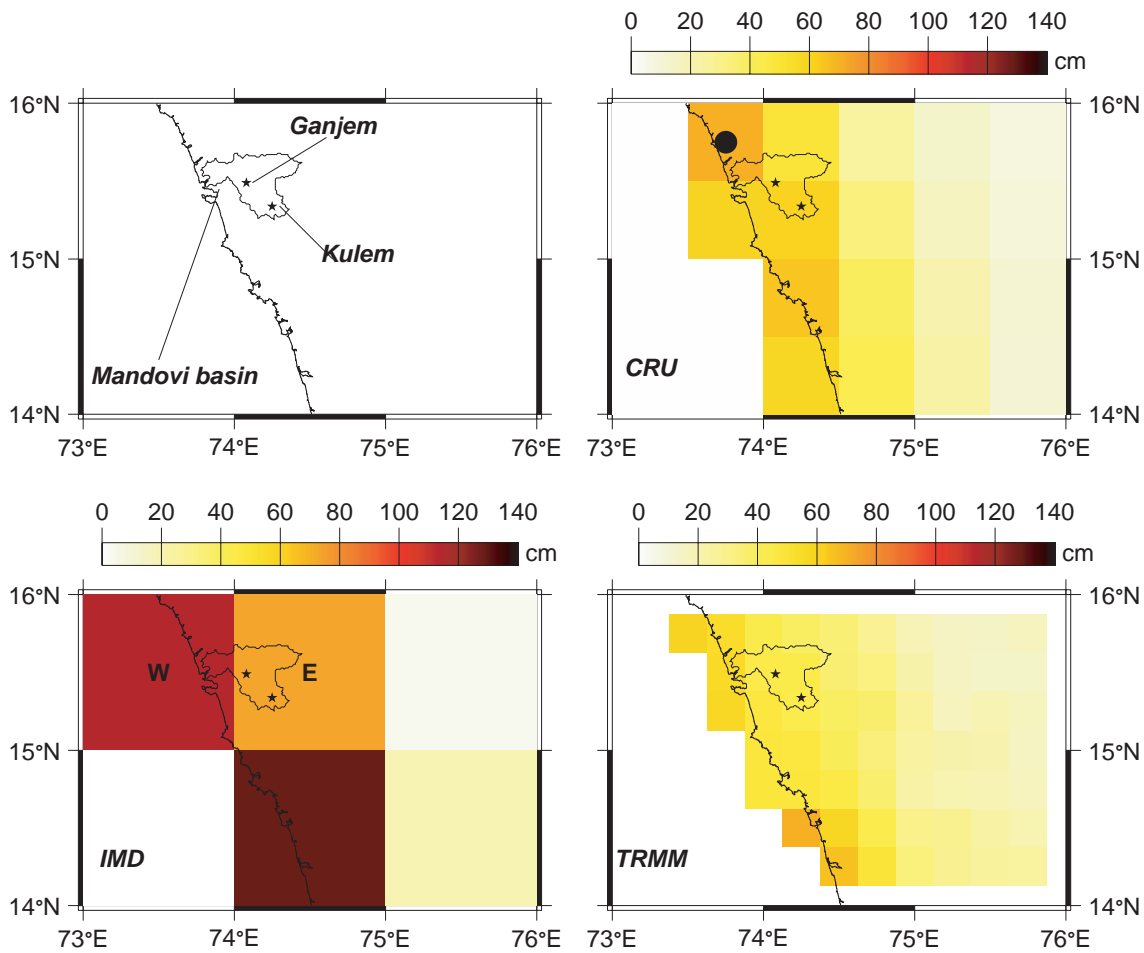


Figure 4

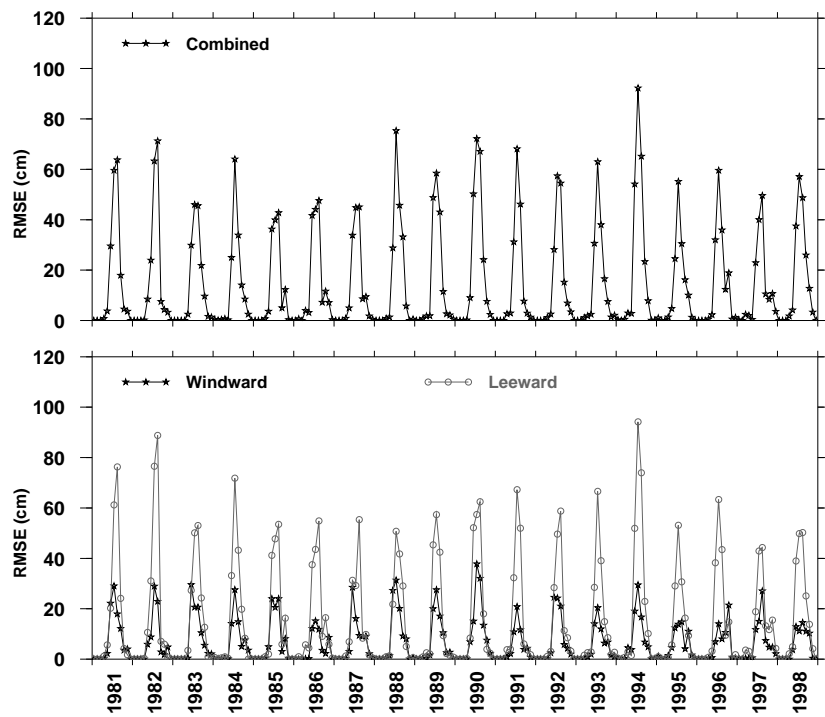


Figure 5

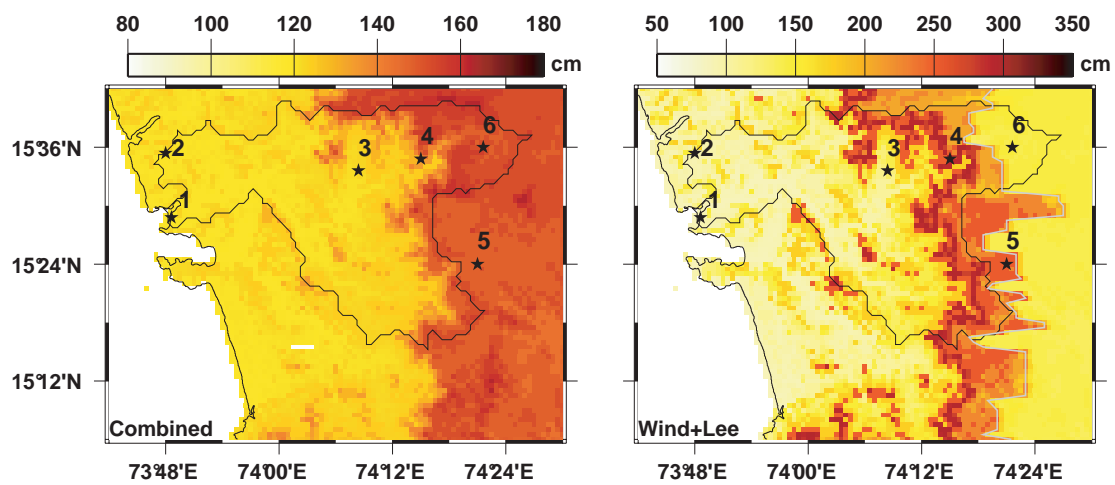


Figure 6

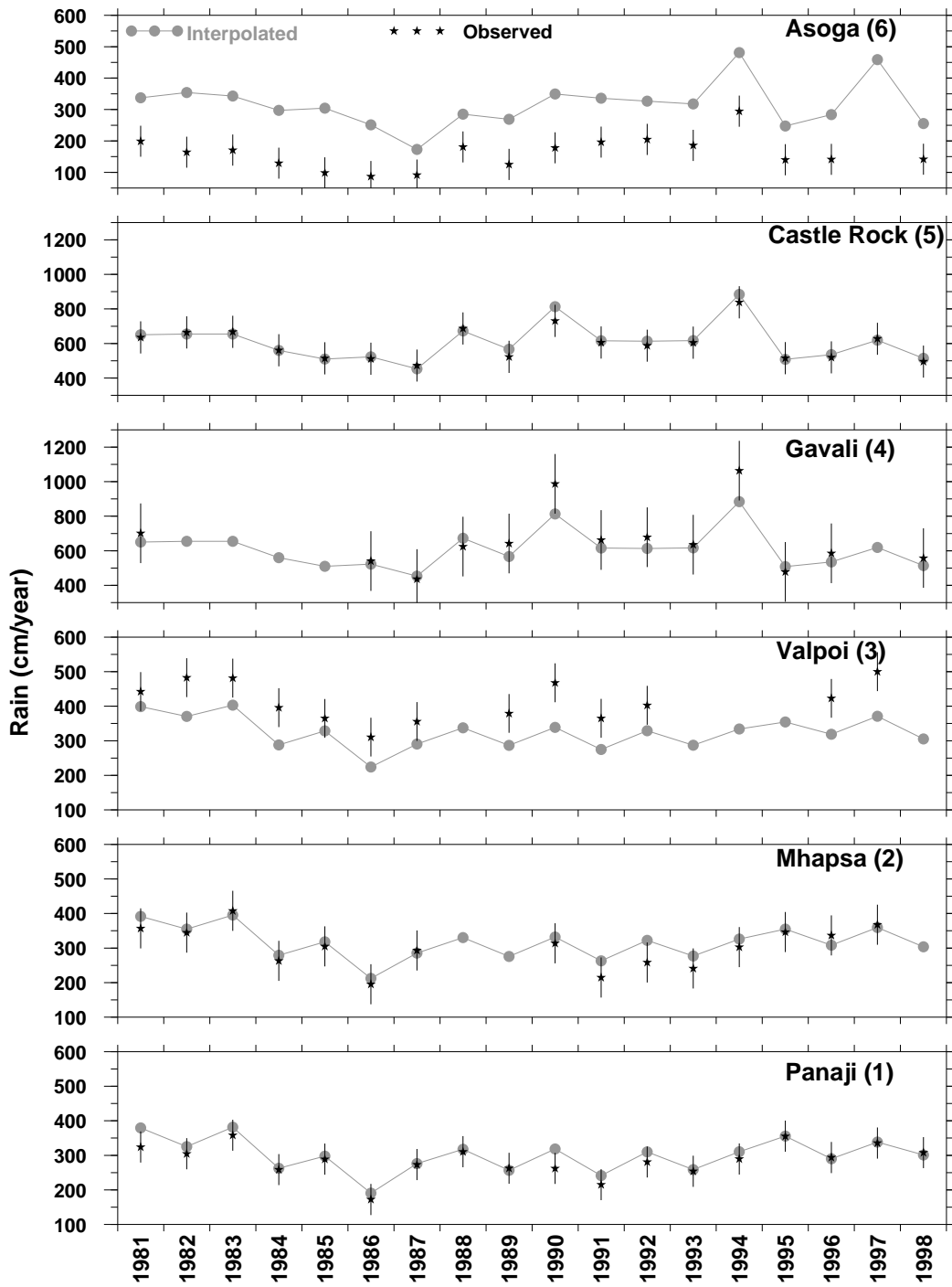


Figure 7

